OBSERVATION OF TWO-PHOTON QUANTUM INTERFERENCE USING ENTANGLED PHOTONS

by

Lee Johnson

A senior thesis submitted to the faculty of

Brigham Young University

in partial fulfillment of the requirements for the degree of

Bachelor of Science

Department of Physics and Astronomy

Brigham Young University

August 2007

BRIGHAM YOUNG UNIVERSITY

DEPARTMENT APPROVAL

of a senior thesis submitted by

Lee Johnson

This thesis has been reviewed by the research advisor, research coordinator, and department chair and has been found to be satisfactory.

Date	Michael Ware, Advisor
Date	Eric Hintz, Research Coordinator
Date	Branton Campbell, Assistant Professor

ABSTRACT

OBSERVATION OF TWO-PHOTON QUANTUM INTERFERENCE USING ENTANGLED PHOTONS

Lee Johnson

Department of Physics and Astronomy

Bachelor of Science

We constructed a two particle interferometer. Using the finished interferometer, we were able to observe two-photon interference using entangled photon pairs produced through parametric down conversion. This phenomenon cannot be explained classically, but demonstrates purely quantum effects, explainable using quantum theory.

ACKNOWLEDGMENTS

I would like to acknowledge David Niemi, Stephany Magelby, and Nathan Terry for the work they have put into this project, which has been ongoing for almost 10 years.

I also wish to thank ORCA for the grant we received, which enabled us to purchase new equipment to aid in data acquisition.

Finally, I would like to thank Dr. Michael Ware for the time he has spent helping troubleshoot this experiment from its initial stages to its final completion, and for the help he has put into this final report.

Contents

List of Figures

Chapter 1

Introduction

1.1 Parametric Downconversion

Over the last 20 years, parametric downconversion has become a commonly used source of correlated photon pairs. In the process of parametric downconversion, a blue or ultraviolet laser (called the pump beam) passes through an optically nonlinear birefringent crystal. A very small percentage of the photons in the incident beam are effectively split into pairs called the signal and idler photons, which share the energy and momentum of the original photon. This process obeys conservation of energy according to the equations

$$\omega_{\mathrm{p}} = \omega_{\mathrm{s}} + \omega_{\mathrm{i}} \tag{1.1}$$

$$\mathbf{k}_{\mathrm{p}} = \mathbf{k}_{\mathrm{s}} + \mathbf{k}_{\mathrm{i}}, \tag{1.2}$$

where ω_{p}, ω_{s}, and ω_{i} are the frequencies of the pump laser, signal photon, and idler photon, respectively, and $\mathbf{k}_{\mathrm{p}}$, $\mathbf{k}_{\mathrm{s}}$, and $\mathbf{k}_{\mathrm{i}}$ are the wave numbers of each. Equations (1.1) and (1.2) are often referred to as phase matching conditions. Generally the polarization of the pump beam must be oriented so that it experiences the ordinary index of refraction in the crystal for downconversion to take place.

Parametric downconversion, or PDC, can be carried out in two ways. In type-I PDC the two downconverted photons are created with parallel polarizations, so Eq. (1.2) becomes

$$\mathbf{k}_{\mathrm{p,o}} = \mathbf{k}_{\mathrm{s,e}} + \mathbf{k}_{\mathrm{i,e}}, \tag{1.3}$$

where "o" and "e" indicate polarization along the ordinary or extraordinary axes of the crystal. In type-I PDC, the photons leave the crystal in a cone, as depicted in Fig. 1.1(a).

In type-II PDC, the two photons are created with orthogonal polarizations, so Eq. (1.2) becomes

$$\begin{aligned} \mathbf{k}_{\mathrm{p,o}} &= \mathbf{k}_{\mathrm{s,o}} + \mathbf{k}_{\mathrm{i,e}} \\ \mathbf{k}_{\mathrm{p,o}} &= \mathbf{k}_{\mathrm{s,e}} + \mathbf{k}_{\mathrm{i,o}}. \end{aligned} \tag{1.4}$$

Since the nonlinear crystal is birefringent, the two photons will experience different indices of refraction and will leave the crystal in two different cones, as depicted in Fig. 1.1(b). In our experiment we used Beta-Barium-Borate (β-$Ba_2B_2O_4$, or BBO) as our crystal, and it was cut to produce type-II PDC with collinear degenerate photons, as depicted in Fig. 1.1(c).

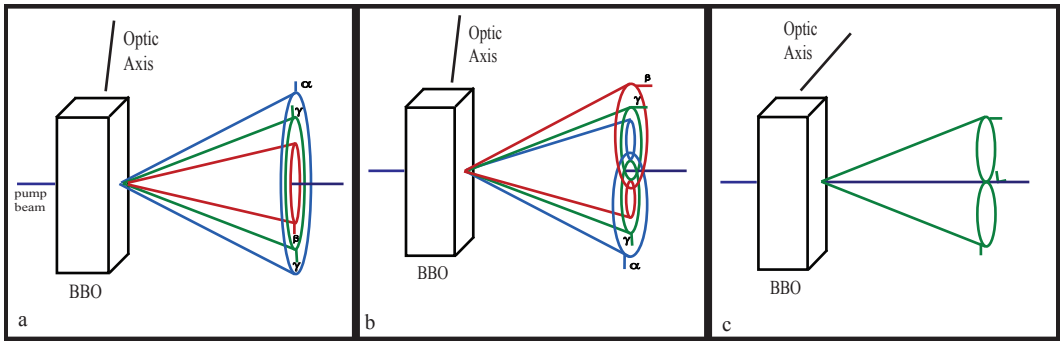

Figure 1.1 a) Type-I PDC. Photons α and β are correlated photons of different frequencies ω_s and ω_i. Photons γ are degenerate. b) Type-II PDC. c) Type-II PDC in which the optic axis of the crystal has been aligned collinear degenerate photon pairs.

1.2 Two Particle Interference

The two photons created through parametric downconversion are like twins: they are created at the same moment and originate from the same point. Moreover, due to the phase matching conditions in Eqs. (1.1) and (1.2), by observing one photon we can instantly determine the qualities of the other. This allows us to construct an entangled state with the two photons. An entangled state is a two-particle state that cannot be expressed as a product of two one-particle states [1].

If we sent two photons into a beam splitter and put detectors on the output arms, there would be four possible outcomes, as illustrated in Fig. 1.2: both could be transmitted (T-T), one could be transmitted while the other is reflected (R-T and T-R), or both could be reflected (R-R). If the two photons are indistinguishable, however, then we can only see three outcomes, since the first two (R-R and T-T) will both appear as synchronous detections on the two outputs of the beam splitter. This can also be set up for two photons propagating collinearly [2] — the only difference then would be that the R-T and T-R cases would be indistinguishable.

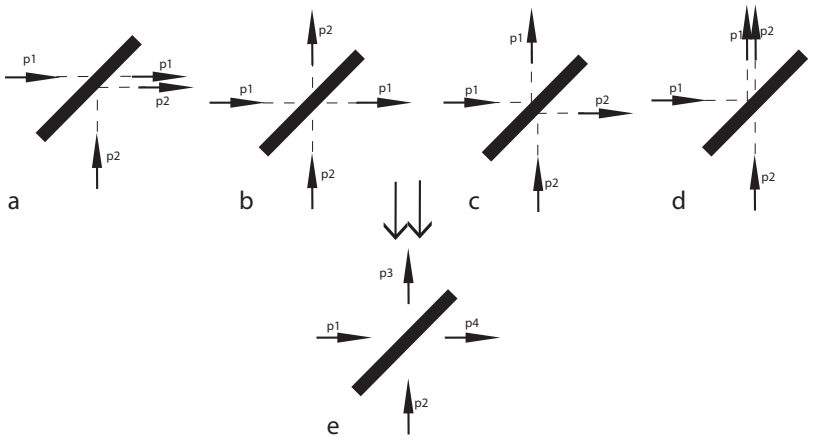

Figure 1.2 (a)-(d) The four possible outcomes of two photons entering a beam splitter. e) The outcome combining (b) and (c) if the two outgoing photons are indistinguishable.

In the example illustrated above, if there is no way, even in principle, to distinguish between the two cases which both result in a synchronous photon detection, then the two photons are entangled. In this case, because the two photons are a single entangled state, then the probabilities of events can interfere. In this setup, the probabilities of T-T and R-R destructively interfere, and thus the probability of a synchronous detection goes to zero. This interference is strictly a quantum phenomenon — it cannot be explained by classical optics.

This interference relies on the two photons being indistinguishable, so any distinguishability eliminates the interference. One example of how we might distinguish between the two cases would be if one of the photons had a slight temporal delay with respect to the other. If this were the case, then we could tell which detector it went to by determining which one triggered second. Likewise, if the two photons have orthogonal polarizations, then we could hypothetically use polarization to determine which detector each photon went to. It doesn't matter whether or not we actually distinguish these properties in our experiment — the fact that in principle we *could* distinguish the two cases will prevent the interference from being observed.

1.3 Previous Work in Research Settings

In 1987 Hong, Ou, and Mandel [3] observed two-particle interference using the experimental setup shown in Fig. 1.3(a). Correlated photon pairs were produced using type-I PDC. The pairs exited the crystal at different angles and were reflected onto a beam splitter. By adjusting the position of the beam splitter, they were able to compensate for any difference in the photons' paths. Their findings can be seen in Fig. 1.3b. Note that the number of coincidence counts drops to zero at the point where distinguishability is completely eliminated.

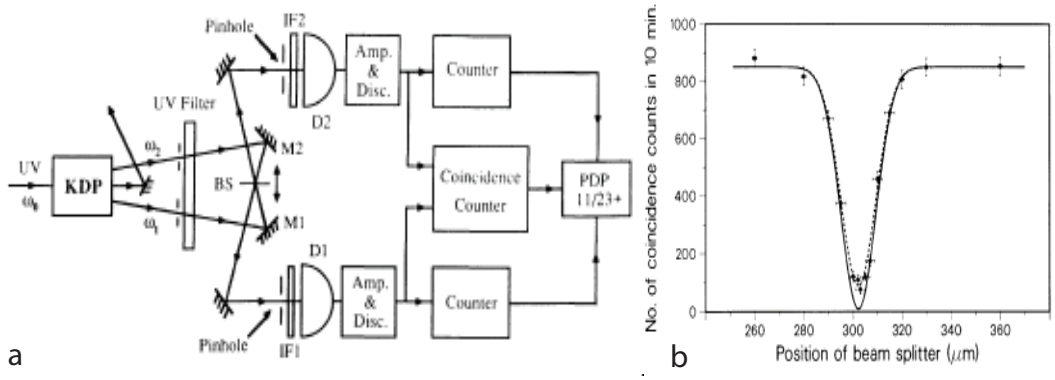

Figure 1.3 a) The experimental setup of Hong, Ou, and Mandel. b) The data they obtained. Both as published by Hong, Ou, and Mandel [3].

In 1995, Sergienko, Shih, and Rubin performed a similar experiment using collinear photons produced through type-II PDC [4], as shown in Fig. 1.4. The pump beam was stopped using mirrors which allowed the downconverted photons to pass. In their setup, because type-II PDC is used, the two photons follow the same path. Distinguishability still arises, however. First, the two photons are distinguishable in principle due to their orthogonal polarizations. Second, because they have orthogonal polarizations, a temporal delay is introduced in the crystal itself due to its birefringence — one photon will travel faster than the other in the crystal. Sergienko et. al. eliminated the first cause of distinguishability by introducing polarizers in front of each detector, oriented at 45°. This destroyed any polarization information from incoming photons before they reached the detectors. They compensated for the temporal distinguishability by inserting thin pieces of quartz after the BBO such that the fast axes of the quartz aligned with the slow axis of the BBO crystal. Coincidence counts were measured as a function of quartz thickness, and the dip characteristic of the interference is observed when the delay introduced by the BBO is compensated for by the quartz (see Fig. 1.4).

The setup of Hong, Ou, and Mandel has the advantage that because it uses type-I

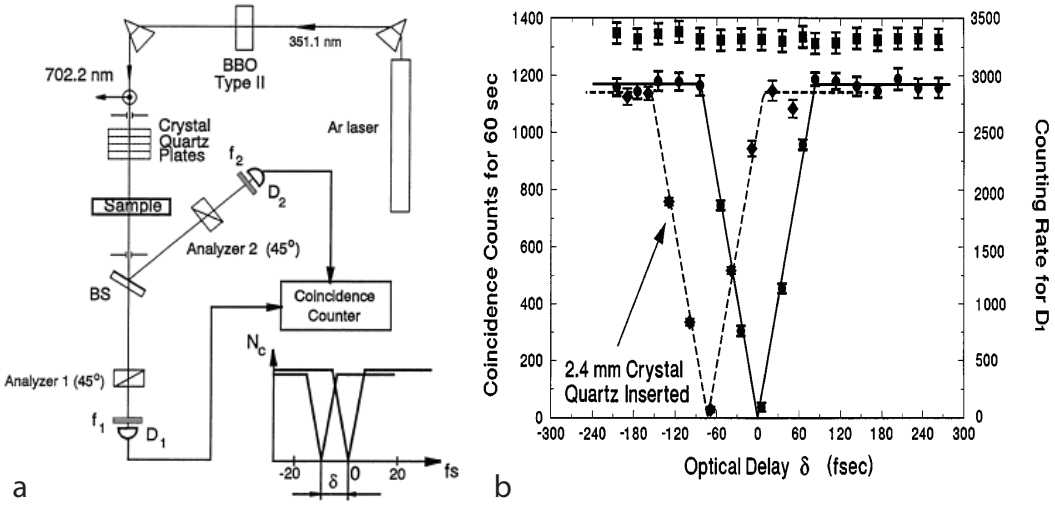

Figure 1.4 a) The experimental setup of Sergienko, Shih, and Rubin [4] b) The results they published.

PDC, no distinguishability is introduced due to differing polarizations. Unfortunately, because the photons leave along different paths, this setup is more difficult to align. The setup of Sergienko et. al. bears the advantage of being easier to align, since the photons propagate collinearly with the pump beam. However, it has the disadvantage that the mirrors used to stop the pump beam will also eliminate a a fraction of the downconverted photons. Furthermore, use of the polarizers to destroy distinguishability eliminates 50% of the downconverted photons on each output of the beam splitter. This results in lower count rates, so longer scans are required to obtain sufficient data to observe interference. At BYU, we decided to use the setup of Sergienko et. al. to observe two particle interference.

1.4 Mathematical Description

The full mathematical description of what is happening is somewhat lengthy. Here we summarize a derivation by Sergienko [4], although a more comprehensive derivation is described by Branning [5]. This derivation was also summarized in Nathan Terry's

thesis [6].

We assume that the photon pair created through type-II PDC travels through a BBO crystal of width L_{BBO}, followed by a delay compensation (in this case quartz) with a thickness of L_q and fast and slow indices of refraction $n_{\hat{s}}$ and $n_{\hat{f}}$. We also assume that the polarizers are oriented at angles θ_3 and θ_4.

We begin with the two-photon state vector emerging from the crystal,

$$|\Psi\rangle = \int \mathrm{d}\omega_\mathrm{s}\delta\left(\omega_\mathrm{s}+\omega_\mathrm{i}-\omega_\mathrm{p}\right)\psi\left(\mathrm{k_s}+\mathrm{k_i}-\mathrm{k_p}\right)a_o^\dagger\left[\omega_\mathrm{s}\mathrm{k}_s\right]a_e^\dagger\left[\omega_\mathrm{i}\mathrm{k}_i\right]|0\rangle. \tag{1.5}$$

The delta function in the above equation represents the phase matching condition for frequency. The phase matching condition for the wave number is not represented with a delta function due to the finite length of the BBO crystal. The function $\psi(\mathrm{k_s}+\mathrm{k_i}-\mathrm{k_p})$ gives the spectral width of the two photon state as

$$\psi(\Delta\mathrm{k}) = \frac{\left(1-\mathrm{e}^{-iL_\mathrm{BBO}\Delta\mathrm{k}}\right)}{iL_\mathrm{BBO}\Delta\mathrm{k}}, \tag{1.6}$$

where $\Delta\mathrm{k} = \mathrm{k_s}+\mathrm{k_i}-\mathrm{k_p}$. We can use a Taylor expansion about the mean down conversion frequency, $\bar{\omega}$, to simplify Eq. (1.6) to

$$\psi(\Delta\mathrm{k}) = \frac{\left(1-\mathrm{e}^{-iv\tau_\mathrm{BBO}}\right)}{iv\tau_\mathrm{BBO}}, \tag{1.7}$$

where v is half the bandwidth of the two-photon state, and τ_BBO is the maximum delay that two photons can obtain in the BBO crystal, given as

$$\tau_\mathrm{BBO} = \left(\left.\frac{\mathrm{dk}_{s,\mathrm{BBO}}}{\mathrm{d}\omega}\right|_{\bar{\omega}} - \left.\frac{\mathrm{dk}_{f,\mathrm{BBO}}}{\mathrm{d}\omega}\right|_{\bar{\omega}}\right)L_{BBO}. \tag{1.8}$$

In Eq. (1.13), $\frac{\mathrm{dk}_{s,f}}{\mathrm{d}\omega}$ is the group delay (inverse of the group velocity) of a pulse of frequency ω in the BBO, polarized along the slow or fast axis.

If we consider a collinear case of the situation shown in Fig. 1.2(e), where two photons enter a beam splitter in arm 1 and leave in arms 3 and 4 (also illustrated in

Fig. 3.6), we can represent the electric fields at detectors 3 and 4 as

$$\begin{aligned} \mathrm{E}_3^{(+)}(t) &= R\cos(\theta_3)\int \mathrm{e}^{-i\omega(t-s)}\left[a_o(\omega)+a_e(\omega)\right]\mathrm{d}\omega \\ \mathrm{E}_4^{(+)}(t) &= T\cos(\theta_4)\int \mathrm{e}^{-i\omega(t-s)}\left[a_o(\omega)+a_e(\omega)\right]\mathrm{d}\omega, \end{aligned} \tag{1.9}$$

where θ_n is the angle of the polarizer at the detector n (which we take to be 45°), s is the optical path length to the detector (which we assume to be the same for both detectors), R and T are the complex reflection and transmission coefficients for the beam splitter (which we assume is 50:50), and $a_o(\omega)$ and $a_o(\omega)$ are annihilation operators. The two-photon wave function after the beam splitter is a combination of the input states $|\psi\rangle$ and $|0\rangle$ and the electric fields in Eqs. (1.9):

$$\begin{aligned} \Psi(t_3,t_4) = & \quad \langle 0|\, E_3^{(+)}(t_3)E_4^{(+)}(t_4)\,|\Psi\rangle \\ = & \quad v_0\mathrm{e}^{\frac{-\sigma_p^2(t_3+t_4)^2}{8}}\left[\Pi(t_3-t_4)-\Pi(-(t_3-t_4))\right], \end{aligned} \tag{1.10}$$

where v_0 is a normalization constant, σ_p is the bandwidth of the Gaussian pump beam, and $\Pi(t)$ is a square function given by

$$\Pi(t) = \begin{cases} 1 & \text{if } 0 \le t \le \tau_{\mathrm{BBO}} \\ 0 & \text{otherwise} \end{cases}. \tag{1.11}$$

In Eq. (1.10), the two square functions in brackets cannot interfere because the first is centered at $\frac{\tau_{\mathrm{BBO}}}{2}$ and the second is centered at $-\frac{\tau_{\mathrm{BBO}}}{2}$. However, if we introduce a quartz delay compensation, then Eq. (1.10) becomes

$$\Psi(t_3,t_4) = v_0\mathrm{e}^{\frac{-\sigma_p^2(t_3+t_4)^2}{8}}\left[\Pi(t_3-t_4+\tau_{\mathrm{q}})-\Pi(-(t_3-t_4)+\tau_{\mathrm{q}})\right], \tag{1.12}$$

where the delay of the quartz, τ_{q} is given by

$$\tau_{\mathrm{q}} = \left(\left.\frac{\mathrm{dk}_{s,\mathrm{q}}}{\mathrm{d}\omega}\right|_{\bar{\omega}} - \left.\frac{\mathrm{dk}_{f,\mathrm{q}}}{\mathrm{d}\omega}\right|_{\bar{\omega}}\right) L_q. \tag{1.13}$$

The two terms in brackets in Eq. (1.12) now overlap completely when $\tau_{\mathrm{q}} = \frac{\tau_{\mathrm{BBO}}}{2}$. The coincidence rate is given by

$$\begin{aligned} \mathrm{R}_c = & \ \tfrac{1}{T} \int \int_0^T \mathrm{dT}_3 \mathrm{dT}_4 \left| \Psi \left(\mathrm{T}_3 - s, \mathrm{T}_4 - s \right) \right|^2 \\ = & \ \mathrm{R}_0 \left[1 - \Lambda \left(\tau_{\mathrm{q}} \right) \right], \end{aligned} \tag{1.14}$$

where $\Lambda \left(\tau_{\mathrm{q}} \right)$ is a triangle function given by

$$\Lambda \left(\tau_{\mathrm{q}} \right) = \begin{cases} \frac{2\tau_{\mathrm{q}}}{\tau_{\mathrm{BBO}}} & \text{if } 0 < \tau_{\mathrm{q}} \leq \frac{\tau_{\mathrm{BBO}}}{2} \\ 2 - \frac{2\tau_{\mathrm{q}}}{\tau_{\mathrm{BBO}}} & \text{if } \frac{\tau_{\mathrm{BBO}}}{2} \leq \tau_{\mathrm{q}} \leq \tau_{\mathrm{BBO}} \\ 0 & \text{otherwise} \end{cases}. \tag{1.15}$$

From Eq. (1.14) we can see that when the quartz compensates for half of the maximum possible delay introduced by the BBO crystal, the coincidence rate should drop to zero.

1.5 Previous Work at BYU

This project was started by Nathan Terry, Stephanie Magelby, and Justin Peatross in 1998 and was the subject of Nathan Terry's masters thesis [6]. Terry constructed our PDC apparatus shown in Fig. 1.5 using a 200mW, 457.9 nm Spectraphysics 2020 Argon-Ion laser incident upon a BBO crystal cut such that its optic axis was 37.2±0.5° from the surface normal. The apparatus produced 916 nm degenerate photon pairs, which exited the crystal collinearly with the pump beam. He also constructed the housing for the photodiodes which were initially used to detect the photons that were produced. He worked mainly to build and characterize the PDC source.

David Niemi continued work on this project a few years later and used it as was the subject of his senior thesis in 2004 [7]. He inserted a polarizing beam splitter

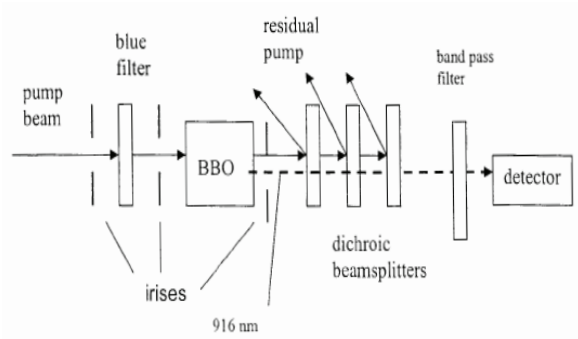

Figure 1.5 The PDC apparatus constructed by Terry [6].

positioned at 45° with respect to the crystal axes and integrated two new commercially packaged avalanche-photodiode single-photon detectors. He also placed two triangular quartz prisms, shown in the setup illustrated in Fig. 1.6(a), to create a variable delay compensation. As the prisms were moved along a translational axis, the thickness of the quartz varied. The photons, after passing through the beam splitter, continued through two polarizers oriented at 45°. They then passed through a 20 nm band pass filter centered at 916 nm (to eliminate uncorrelated noise) and arrived at two collectors. The two collectors focused the incident photons into multimode fiberoptic cables, which delivered them to the photon detectors. Synchronous detections were measured by connecting both detectors to a computer.

The two detectors used emit a 5 V, 40 ns pulse upon detection of a photon. One detector was connected using a short cable, the other using a much longer cable. The signal from the first detector arrived first and triggered the computer to begin looking for a signal from the second detector. For this reason, the detectors are commonly referred to as "start" and "stop" detectors. If a signal arrived from the stop detector at the time corresponding to the cable delay, then the computer counted the event as a "coincidence", indicating a positive detection of a correlated photon pair.

Niemi was able to measure coincidences with the setup shown, but he was unable to

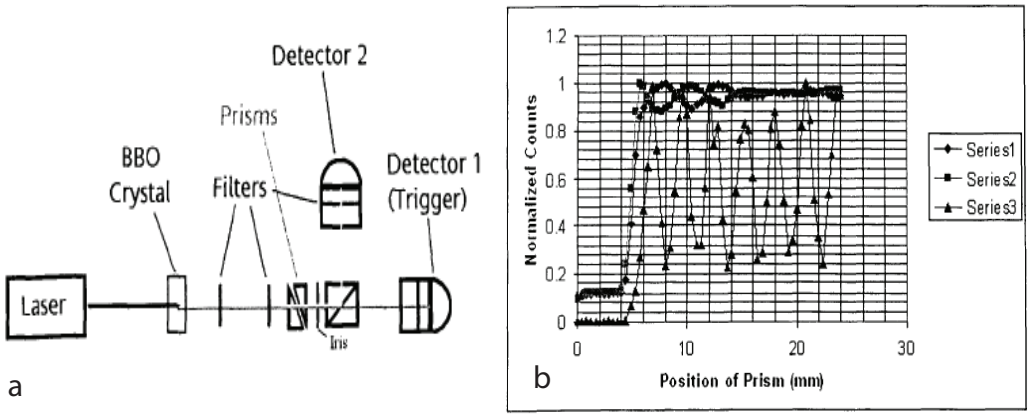

Figure 1.6 Setup used by Niemi to observe correlated photon pairs [7].

observe two-photon interference. Instead, he observed oscillations in the coincidence rates which appeared to correspond to classical interference, as shown in Fig. 1.6.

Chapter 2

Experimental Setup

2.1 Equipment Changes

Our first task when we began this project was to reconstruct the setup used by Niemi to detect correlated photon pairs. In the process of reconstructing the apparatus, we made numerous modifications and improvements.

2.1.1 Beam splitter

To make alignment simpler, the first change we made to the setup was to replace the polarizing beam splitter with a non-polarizing beam splitter, similar to many present research groups. The introduction of a non-polarizing beam splitter allowed us to align the equipment without having to worry about the orientation of the beam splitter with respect to the axes of the crystal.

2.1.2 Translational stages

The second change that we made to the setup of Niemi was to obtain x-y translational stages for each collector. This made the alignment process easier and more precise,

since the detectors' positions could be adjusted with micrometers. We could also record the configuration of the detectors before making changes to their positions, allowing us to quickly recover a previous alignment. The collectors were mounted to allow tip-tilt adjustment, so altogether we could adjust each collector along four axes.

2.1.3 Electronics

The most significant changes that we made in the setup were to the electronics that measured the counts. In the setup used by Niemi, each pulse generated by a detector was split and sent both to an individual counter to measure singles counts and and to a separate circuit used to measure coincidences. He used the two counters on a National Instruments PCI-MIO-16E-4 data acquisition board to measure singles counts and sent the signals into either an Ortec 414 Fast Coincidence module or a Stanford Research Systems SR430 Multichannel Binner/Averager to measure coincidences.

Initially we looked for another way to measure singles counts, since the method used by Niemi was software gated, meaning that the software determined when measurement began and ended. To obtain reliable data, it is important that we be able to compare coincidence rates taken at various crystal thicknesses, so we need to have an accurate measurement of the amount of time that detection is underway (often called the gate time or gate width). Determining the gate width with software alone is inaccurate, since any fluctuation in the processor performance could make our measurement proceed for a longer or shorter interval than specified and thus give us a higher or lower count rate. Accuracy is important for both singles and coincidence counts. To positively identify the occurrence of two-particle interference, we watch for the coincidence counts to drop *while the singles counts do not vary*, as seen in the data collected by Sergienko et. al., depicted in Fig. 1.4(b). If we observe a drop in our coincidence counts and there is also a drop in our singles counts, it could only be an

intensity fluctuation due to something like a smudge on the quartz at that position.

We first attempted to obtain an accurate gate by using two Racal Dana counters, which could be voltage gated. We used the National Instruments board to generate a precisely defined digital pulse which enabled counting when the voltage was high. However, since communication with the counters over the GPIB interface was both slow and unreliable, we eventually looked for another solution.

We also looked for another way to measure coincidences. Initially we used the Ortec 414 Fast Coincidence module used by Niemi, but this had the disadvantage that it registered a coincidence any time the two detectors fired within a certain window of time: it didn't distinguish between the start and stop counters, and it didn't eliminate signals that arrived too closely spaced. For example, if two signals arrived 5 ns apart, but our delay cable separated synchronous pulses by 60 ns, it would still count it as a coincidence, since it arrived within the time window. The SR430 multichannel binner used by Niemi overcame this difficulty by providing a histogram of stop count delays (depicted in Fig. 2.1), but it also communicated over a GPIB interface, and it required about 250 μs to register a single coincidence. If two pairs of correlated photons arrived too closely spaced, one would not be measured, so this limited the number of coincidences we could observe.

We overcame both of these problems by obtaining a National Instruments PCI-6602 counter/timer board. This board has eight counters and an internal 80 MHz clock. We sent the signals from the two detectors into two of the counters. The counters synchronously counted the internal clock and, at the arrival of a pulse, appended the current value of the internal clock to a growing array. At the end of our gate period we had two arrays of timestamps in which each element corresponded to the arrival of a photon from that detector. While we could not voltage gate this hardware, the fact that we could timestamp the signals made it unnecessary. We

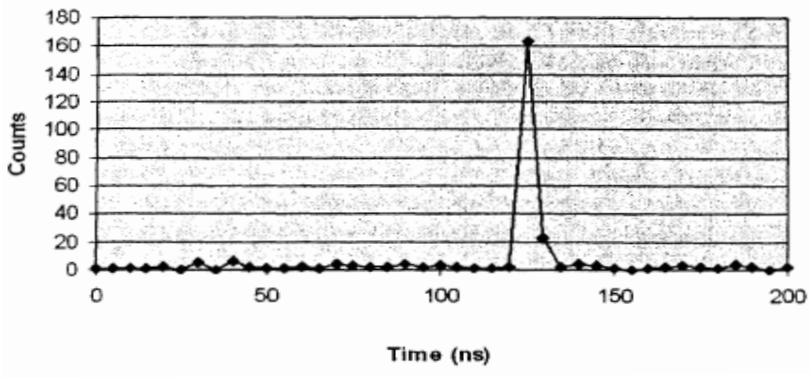

Figure 2.1 A histogram created by the SR430 multichannel binner in the setup of Niemi [7]. The binner begins measuring upon arrival of a pulse from the start detector and places any signals from the stop detector in a bin according to their time of arrival.

achieved an accurate gate by allowing the scan to proceed slightly beyond our desired gate period and then truncating any elements whose timestamps were over the gate time. We were then able to construct a histogram from the two arrays, as shown in Fig. 2.2.

The histogram we were able to obtain allowed us to more accurately determine the number of coincidence counts we were observing. Not only were we able to precisely determine the number of counts arriving at the delay specified by the stop counter's cable length (the area of peak "a" in Fig. 2.2), but we were also able to measure the amount of background noise to subtract it from the total counts (point "b" in Fig. 2.2). The 12.5 ns resolution provided by the 80 MHz internal clock of the PCI-6602 board wasn't as nice as the 5 ns resolution provided by the SR430 binner, but it communicated directly with the computer over the PCI bus and it was more convenient to use. It also eliminated the need to split the signals, since singles and coincidences were measured with the same hardware. Since splitting a 50 ns pulse created significant reflections in the cable, this eliminated noise and cleaned up our signal.

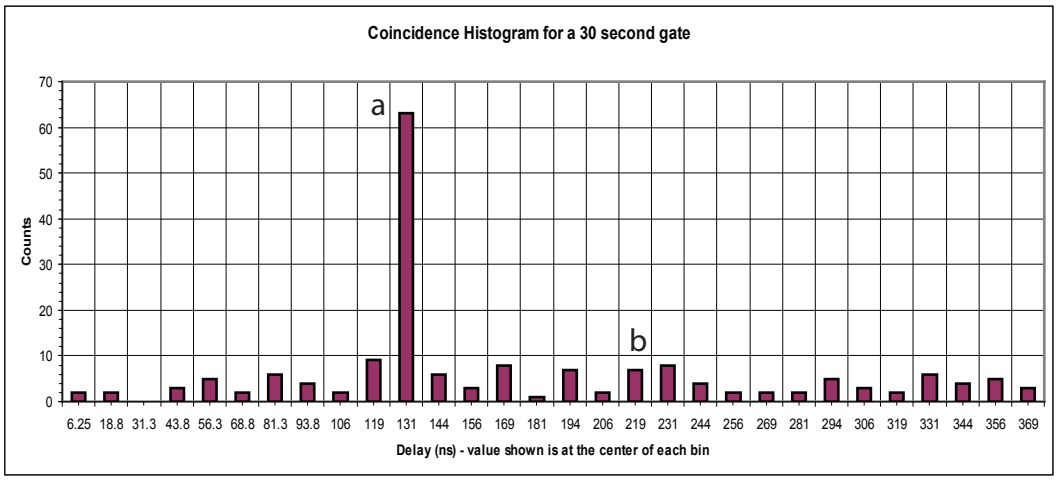

Figure 2.2 Our histogram obtained using the PCI-6602, showing stop delay of about 131 nanoseconds, as indicated by the location of the peak (a). Random photons which are closely spaced but aren't correlated pairs, shown as (b), are averaged and subtracted from the coincidence peak.

2.2 Programming Changes

In addition to the improvements that we made regarding the equipment, alignment, and circuitry of the setup, we also made notable improvements to the software which collects and manages the data during the scans. Dr. Ware wrote an application specifically designed to collect coincidence data while working at NIST, and we have spent considerable time adapting that software to run this setup. This required writing code to run each of the devices, but the advantage is that now the scanning process is fully automated. To run a scan is now very simple, as it is only necessary to specify the gate period, the increments to move the quartz prisms, and how many samples (gates) we want to measure at each position. The software performs the whole scan, displays the data, calculates the true coincidences, and saves everything to a file. These improvements will be very useful in the future, when students may operate the setup for walk-in labs for the Optics class.

The only thing specifically worth noting in our incorporation of this software is

the implementation of the PCI-6602 board. When we began using the 6602 board, we discovered that it did have a limitation in the rate at which it could timestamp single photon pulses from a detector. The data transfer rate from the buffer is limited to about 245k samples/sec [8], meaning that if a detector sent two pulses that were spaced less than about 4 μs apart, the board overwrote the data in the buffer, returned an error, and immediately halted the scan. This could happen several times per second, especially if the intensity of the pump beam is high and more photons are hitting the detectors, so we were unable to obtain more than a second's worth of data before our scan was stopped. The detectors themselves also have a small chance (less than 1 percent) of generating an after-pulse just after sending a signal, as shown in Fig. 2.3 [9], which would effectively appear as two closely spaced photons and cause the same error.

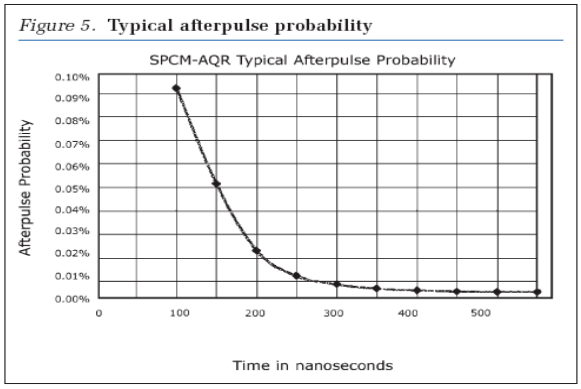

Figure 2.3 A graph from the datasheet for the photon detectors [9], showing the probability of a detector randomly generating an afterpulse just after sending a pulse corresponding to a photon detection.

This error didn't limit coincidence detection, since it only happened when two pulses arrived too close together on the same channel — the pulses from two photons of a correlated pair would travel to separate counters and be stored in separate buffers. However, the random nature of photon arrivals combined with the possibility of after-pulse generation made it impossible to eliminate this error by changing things in our

setup. We had to compensate for the error entirely through programming so that the scan would continue while still keeping an accurate gate period.

We overcame this difficulty by resetting the timestamping process each time such an error occurred. This means that rather than ending up with a final timestamp array whose elements steadily increased in value as depicted in Fig. 2.4(a), we got a final timestamp array similar to Fig. 2.4(b), with sporadic drops corresponding to random arrivals of photons that were too closely spaced. From the initial data, however, we can reconstruct an accurate array after the scan by taking the last timestamp value before an error and adding it onto all subsequent entries. This correction process adds a little bit of post-scan processing time, but it doesn't alter the accuracy of our data measurably.

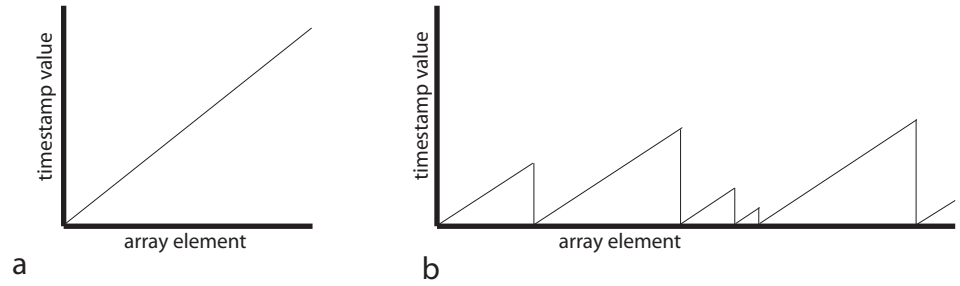

Figure 2.4 a) The expected timestamp arrays, whose elements have increasing values. b) A timestamp array with drops corresponding to buffer errors.

2.3 Present State of Apparatus

With our current setup, illustrated in Fig. 2.5, we are able to consistently observe correlated photon pairs at a rate of about 2-3 counts/second. These rates are sufficient to observe interference with a long enough gate period. To test for interference, we ran scans with a 30 second gate time and typically took about 20 of these 30 second samples at each wedge position.

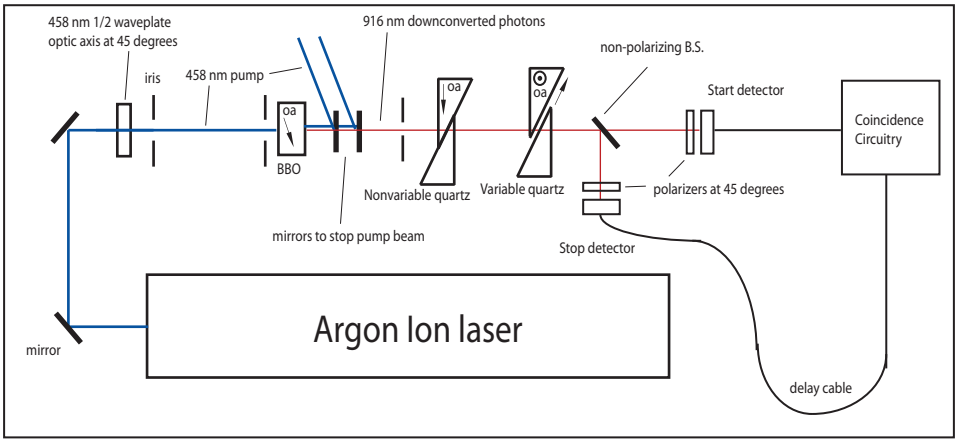

Figure 2.5 Diagram of our experimental setup, viewed from above.

2.4 Expected Values

To calculate the position of the quartz prisms at which we would expect to see the lowest point of our interference dip, we must calculate the delay introduced by the BBO crystal and the thickness of quartz required to eliminate that delay. The delays created by the two crystals will therefore be equal to each other, save that one will have its fast axis rotated 90° to align with the slow axis of the other, so that their delays cancel rather than add. The time delay introduced between two orthogonally polarized photons by a birefringent crystal is

$$\begin{aligned} \Delta t &= t_s - t_f \\ &= \left(\frac{1}{u_s} - \frac{1}{u_f}\right)\Delta x, \end{aligned} \tag{2.1}$$

where Δx is the thickness of the crystal and u_s and u_f are the group velocities for the two polarizations, given by

$$u = \left(\frac{\mathrm{dk}}{\mathrm{d}\omega}\right)^{-1} \tag{2.2}$$

and

$$k(\omega) = \frac{\omega \mathrm{n}(\omega)}{\mathrm{c}}. \tag{2.3}$$

In the above equation, n(ω) is the index of refraction of the medium, and is dependent on both frequency and polarization. Since we determined in section 1.4 that the deepest part of our dip should occur at a quartz thickness compensating for half of the delay introduced by the BBO, we set up Eq. 2.1 for both crystals as

$$\Delta x_{\mathrm{q}}(\frac{1}{u_{\mathrm{q},s}} - \frac{1}{u_{\mathrm{q},f}}) = \frac{1}{2}\Delta x_{\mathrm{BBO}}(\frac{1}{u_{\mathrm{BBO},s}} - \frac{1}{u_{\mathrm{BBO},f}}), \tag{2.4}$$

and the required thickness of the quartz is

$$\Delta x_q = \frac{1}{2}\Delta x_{\mathrm{BBO}}\frac{(\frac{1}{u_{\mathrm{BBO},s}} - \frac{1}{u_{\mathrm{BBO},f}})}{(\frac{1}{u_{\mathrm{q},s}} - \frac{1}{u_{\mathrm{q},f}})}. \tag{2.5}$$

Since the optic axis of the quartz is parallel to the plane of incidence, the indices of refraction experienced by the photons are simply the indices of refraction along the ordinary and extraordinary axes,

$$\begin{aligned} n_{q,s} &= n_{q,e} \\ n_{q,f} &= n_{q,o}. \end{aligned} \tag{2.6}$$

$n_{q,o}$ and $n_{q,e}$ can be calculated at a particular wavelength using the Sellmeir equations for quartz [10]:

$$\begin{aligned} n_{q,e}(\lambda) &= \sqrt{2.35728 - 0.0117\lambda^2 + \frac{0.0105}{\lambda^2} + \frac{0.1341e^{-3}}{\lambda^4} - \frac{0.4454e^{-6}}{\lambda^6} + \frac{0.5924e^{-7}}{\lambda^8}} \\ n_{q,o}(\lambda) &= \sqrt{2.3849 - 0.0126 * \lambda^2 + \frac{0.0108}{\lambda^2} + \frac{0.1652e^{-3}}{\lambda^4} - \frac{0.1947e^{-5}}{\lambda^6} + \frac{0.9365e^{-7}}{\lambda^8}}., \end{aligned} \tag{2.7}$$

where λ is the wavelength of the light in a vacuum, expressed in μm. Inserting Eqs. (2.3) and (2.7) into Eq. (2.2) and making the appropriate substitution of frequency ω for wavelength ($\lambda = \frac{2\pi c 10^6}{\omega}$, since λ is the wavelength in micrometers), we find the group velocities in quartz for light polarized along the slow and fast axes to be $u_{\mathrm{q},s} = 1.55111\mathrm{c}$ and $u_{\mathrm{q},f} = 1.56059\mathrm{c}$, respectively.

The BBO crystal, however, is cut such that its optic axis is $\phi = 37.2 \pm 0.5°$ from the incident plane. This means that the two photons will experience fast an slow indices of refraction given by [11]

$$\begin{aligned} n_{BBO,f} &= n_{BBO,o} \\ n_{BBO,s} &= \frac{n_{BBO,o} n_{BBO,e}}{\sqrt{n_{BBO,o}^2 sin(\phi)^2 + n_{BBO,e}^2 cos(\phi)^2}}, \end{aligned} \tag{2.8}$$

where $n_{BBO,o}$ and $n_{BBO,e}$ are given by the Sellmeir equations for BBO [12]:

$$\begin{aligned} n_{BBO,o}(\lambda) &= \sqrt{2.7359 + \frac{0.01878}{\lambda^2 - 0.01822} - 0.01354\lambda^2} \\ n_{BBO,e}(\lambda) &= \sqrt{2.3753 + \frac{0.01224}{\lambda^2 - 0.01667} - 0.01516\lambda^2} \end{aligned} \tag{2.9}$$

Again, combining Eqs. (2.2), (2.3), (2.8), and (2.9) and and making the appropriate substitution of frequency for wavelength, we find the group velocities in BBO along the slow and fast axes to be $u_{\mathrm{BBO},s} = (1.63212 \pm 0.00010)$c and $u_{\mathrm{BBO},s} = 1.67850$c. The uncertainty in $u_{\mathrm{BBO},s}$ is due to the uncertainty in the angle of the optic axis of the crystal. Using a BBO thickness of 0.5 mm with the values of the group velocities obtained for quartz and BBO, we can calculate the expected quartz thickness from Eq. (2.5) to be

$$\begin{aligned} \Delta q_x &= (0.25mm) \frac{(\frac{1}{1.63212 \pm 0.00010} - \frac{1}{1.67850})}{(\frac{1}{1.55111} - \frac{1}{1.56059})} \\ &= 1.2237 \pm 0.0027mm. \end{aligned} \tag{2.10}$$

As we see above, we expect the lowest part of our dip to be at a quartz thickness of about 1.22 mm. The uncertainty in the cut of the crystal will cause a negligible difference in our expected quartz thickness. Since the adjustable prism is 30° triangles, moved along its hypotenuse, this thickness would correspond to a translational position of $\Delta y = \frac{1.22\mathrm{mm}}{\sin(30°)} \approx 2.44\mathrm{mm}$.

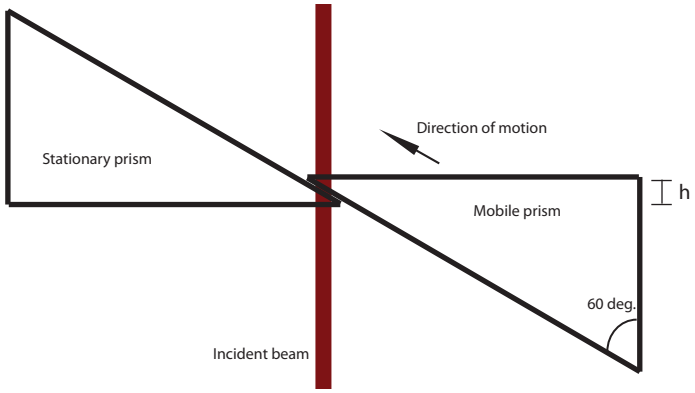

Figure 2.6 The magnitude of the delay compensation is varied by holding one quartz prism fixed while the other is moved along the its hypotenuse. The minimum thickness of the quartz, h, is determined by the beam width.

2.5 Setup Changes

Since we predicted such a small value for the thickness at which our interference will occur, it was necessary to modify our experimental design slightly. It is impractical to try to observe coincidences at a crystal thickness as small as that found in Eq. (2.10), since the beam itself has a finite beam width, and therefore any thickness smaller than that illustrated in Fig. 2.6 will result in part of the beam emerging at a significantly different angle (since it would fail to pass through both prisms). We begin our scans with a thickness of about 3-4 mm of quartz in the downconverted beam, so essentially we would fail to observe the expected interference. This is most likely the reason that Niemi failed to observe interference — due to a miscalculation they expected the dip to appear at a greater quartz thickness than that found in Eq. (2.10).

To overcome this problem, we inserted a second pair of prisms at a fixed thickness upstream from variable-thickness prisms. The second set of prisms had its optic axis oriented 90° from the optic axis of the variable prisms, so its fast axis was aligned with the fast axis of the BBO and it *increased* the original delay between the two photons. We set the thickness of the fixed pair of prisms to about 7.9 mm, so our

new expected thickness for the variable quartz prisms would be

$$\Delta x_{q,variable} = -\Delta x_{BBO}\frac{(n_{BBO,s} - n_{BBO,f})}{(n_{q,s} - n_{q,f})} + \Delta x_{q,fixed} = 1.22\text{mm} + 7.9\text{mm} = 9.18\text{mm}. \tag{2.11}$$

Since the quartz prisms are aligned by hand on the translational stage, we don't know the exact thickness of the delay, but the above value gives us an approximate range in which to look for our interference dip. Since the quartz prisms are 30° triangles, this thickness will occur at a translational position of about 18.4 mm (the prism's position is moved along the hypotenuse). We start our scan with the variable prisms already in the beam and with a thickness of about 2 mm, so we would expect our dip to occur at a translational position of about $\Delta y = \frac{9.18\text{mm}-2\text{mm}}{\sin(30°)} \approx 14\text{mm}$.

Chapter 3

Results

3.1 Observed Interference

3.1.1 First setup

After inserting the second, stationary pair of prisms into the beam as depicted in Fig. 2.5, an interference dip is clearly visible at about 12 mm, shown in Fig. 3.1.

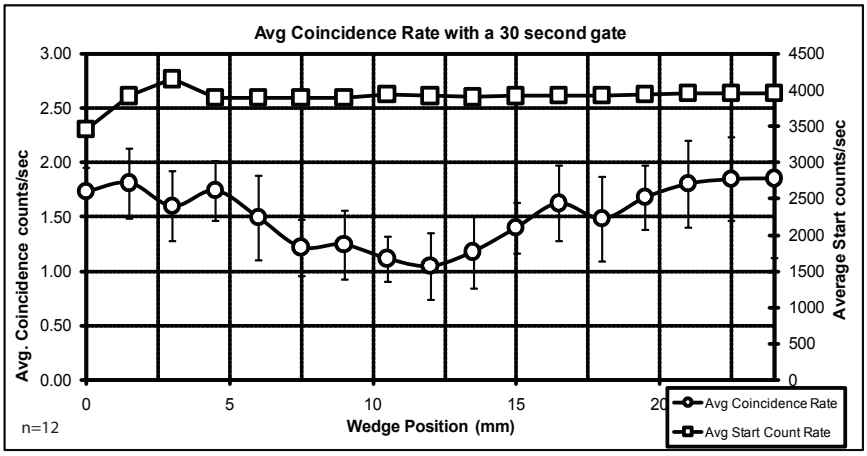

Figure 3.1 The coincidence count rate (lower line) shows a significant drop ($P \leq 0.01$), whose lowest point appears to be around 12 mm. We can see that the singles count rate remains constant.

The observed data clearly indicates interference of the type that we are hoping to observe, but the coincidence rates only drop about 45% at the lowest part of the dip. Our data is also not as clean as we would prefer - we see fluctuations in the average coincidence rate at unexpected positions on the plot, such as those at 4.5 mm, 7.5 mm, and 18 mm.

The messiness of the graph can mostly be attributed to statistical noise. Since we have such a low count rate ($\sim$ 2 counts/sec, compared to the 20 counts/sec observed by Sergienko et. al. [4], shown in Fig. 1.4b), noise becomes a big problem. While we subtract off the average noise to give us a more accurate value of the true coincidences at each point, the data still shows more variation than it would if there were less noise. We could reduce the noise by increasing our coincidence count rate or by taking more samples at each wedge position.

The fact that our coincidence rate doesn't dip down to zero can be explained by a combination of factors. After obtaining the data above, we referred to the data sheet for the beam splitter and found that with our setup it isn't a true 50:50 beam splitter, since the incident light is "s" and "p" polarized with respect to the beam splitter. By looking at Fig. 3.2, we can see that at 916 nm the beam splitter really behaves

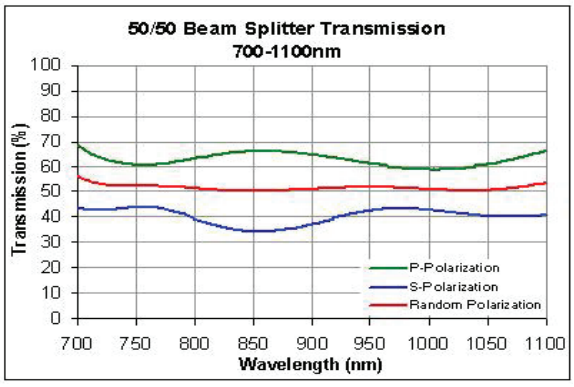

Figure 3.2 A graph from the data sheet for the beam splitter showing the transmission coefficients at various wavelengths [13].

more like a 64:36 beam splitter for "s" and "p" polarized light. Since the percentage reflected or transmitted is polarization dependent, this introduces a certain degree of distinguishability.

Another factor that contributes to the dip not dropping to zero can be seen when we set both polarizers horizontally, as shown in Fig. 3.3. Since the two photons are orthogonally polarized, turning both polarizers to 0° should cause our coincidences to disappear — but it does not. The most likely explanation for this is that our photons are becoming elliptically polarized in one of the birefringent media, most likely due to a misaligned optic axis. To minimize this effect, we placed one of the polarizers upstream of the BBO and adjusted it until we got a minimum (i. e. so that it blocked the pump beam). Since the beam at that point was vertically polarized, we assumed then that the polarizer was perfectly orthogonal to the beam. We then placed the polarizer after the BBO and adjusted the BBO until we got a minimum, indicating that the BBO was aligned so that the polarization of the pump beam was completely ordinary.

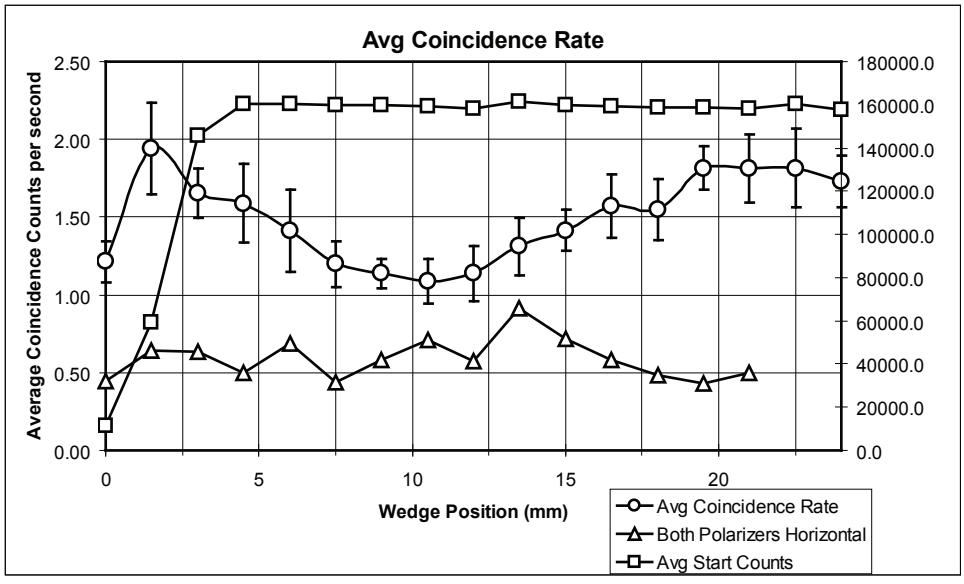

Figure 3.3 A graph showing our dip, but with a corresponding scan taken with both polarizers set at 0° (triangles).

After this procedure we are fairly certain that the downconverted photons leaving the BBO with vertical and horizontal polarizations are in the same basis as the pump. The most likely place where it would pick up ellipticity, therefore, is in the variable quartz delay. We were able to align the fixed-width quartz using the same process as the BBO crystal, since both prisms were on a tip-tilt stage together, but the variable quartz prisms are on separate tip-tilt mounts. The job of aligning them is much more difficult, since the prisms could be misaligned with the BBO or with each other, or both. When we adjusted the alignment of the variable delay prisms, we were unable to get our dip any lower or eliminate the coincidences that are present with both polarizers at 0°.

3.1.2 Second setup

The first solution we sought to make the dip go lower was to use only one polarizer, placed before the beam splitter and set at 45°, as shown in Fig. 3.4. This destroys the polarization distinguishability for both photons and also eliminates any elliptical polarization and make it so that the photons were equally "s" and "p" with respect to the beam splitter. Placing a polarizer before the beam splitter produced the graph in Fig. 3.5, which shows a distinct peak rather than a dip.

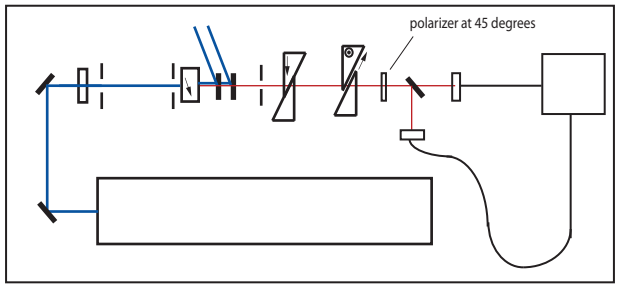

Figure 3.4 Our second setup, with one polarizer in front of the beam splitter, set at 45°.

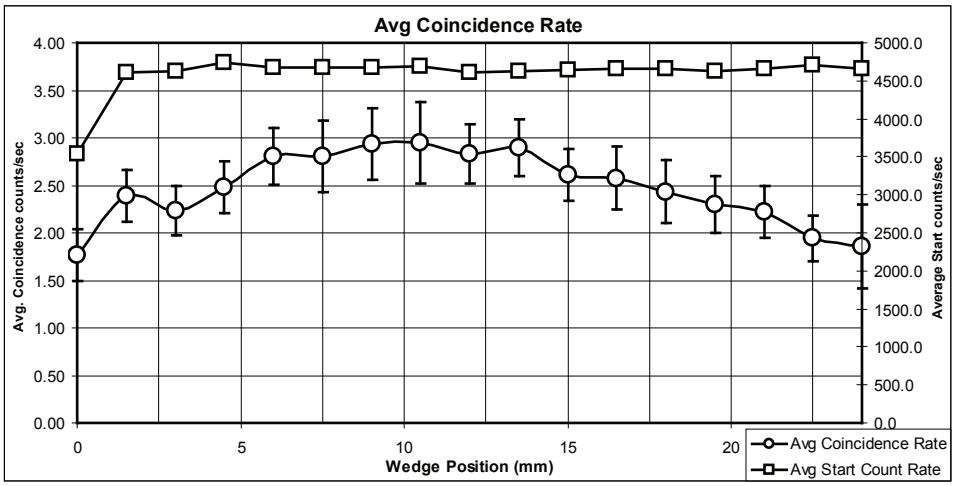

Figure 3.5 Data taken with the second setup.

Rather than the probability of a synchronous detection going to zero, the probability of the photons going to the same detector has gone to zero, while the probability of them splitting has gone to 1.

Mathematically, this is much simpler to explain than the case in setup 1. Since the two photons have the same polarization before they hit the beam splitter, the derivation more closely resembles that for the setup of Hong, Ou, and Mandel with type-I PDC. The only difference is that both photons enter the beam splitter from the same input arm as shown in Fig. 3.6, rather than from different ones as shown in Fig. 1.2. The derivation is the same as that in R. Louden's book [14], up to the expression of the two photon state at the beam splitter:

$$|(2_1, 0_2)\rangle = \int dt \int dt' \beta\,(t, t')\, \hat{a_1}^\dagger(t) \hat{a_1}^\dagger(t')\, |0\rangle. \tag{3.1}$$

In the above equation, the notation on the left side indicates that two photons are entering arm one of the beam splitter and none are entering arm two. The two terms $\hat{a_1}^\dagger(t)$ and $\hat{a_1}^\dagger(t')$ are creation operators acting on the vacuum state $|0\rangle$ and indicating any temporal separation between the photons (photon one arrives at t, photon two at t'). Using the reflection and transmission coefficients for the beam splitter, we

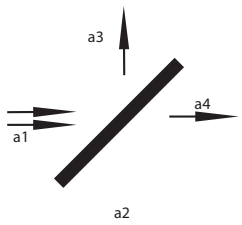

Figure 3.6 Two particles entering a beam splitter with the same polarization and along the same path.

can substitute the creation operators for the input arm of the beam splitter with operators for the output arms with the equation

$$\hat{a_1}^\dagger = R\hat{a_3}^\dagger + T\hat{a_4}^\dagger, \tag{3.2}$$

where $\hat{a_3}^\dagger$ and $\hat{a_4}^\dagger$ are creation operators for the output arms three and four. Substituting Eq. (3.2) into Eq. (3.1) and rearranging yields

$$\begin{aligned} |(2_1, 0_2)\rangle = \quad & \int dt \int dt' \beta\left(t, t'\right) \{R^2 \hat{a_3}^\dagger(t)\hat{a_3}^\dagger(t') + T^2 \hat{a_4}^\dagger(t)\hat{a_4}^\dagger(t') \\ & + RT\left[\hat{a_3}^\dagger(t)\hat{a_4}^\dagger(t') + \hat{a_4}^\dagger(t)\hat{a_3}^\dagger(t')\right]\} |0\rangle , \end{aligned} \tag{3.3}$$

which after interchanging the time variables becomes

$$\begin{aligned} |(2_1, 0_2)\rangle = \quad & \int dt \int dt' \{RT\left[\beta\left(t, t'\right) - \beta\left(t', t\right)\right]\left[\hat{a_3}^\dagger(t)\hat{a_4}^\dagger(t')\right] \\ & + \tfrac{1}{2}\left[R^2\beta\left(t, t'\right) + T^2\beta\left(t', t\right)\right]\left[\hat{a_3}^\dagger(t)\hat{a_3}^\dagger(t') + \hat{a_4}^\dagger(t)\hat{a_4}^\dagger(t')\right]\} |0\rangle . \end{aligned} \tag{3.4}$$

The above equation is the same as that derived by Louden for two particles entering different inputs of the beam splitter, except that the the two terms in brackets containing creation operators for the outputs have changed places, as has the factor of 1/2. The first term containing $\hat{a_3}^\dagger(t)\hat{a_4}^\dagger(t')$ corresponds to simultaneous detection on both outputs: a coincidence. The second term containing $\hat{a_3}^\dagger(t)\hat{a_3}^\dagger(t') + \hat{a_4}^\dagger(t)\hat{a_4}^\dagger(t')$ corresponds to both photons traveling through either output three or four. With a detector capable of showing "doubles" counts, this outcome can actually be observed.

Both cases above can be solved for separately to give probability amplitudes. If interference was not present, then each of the four possible outcomes would have an equal probability of occurring - there would be a 25% chance of both photons exiting through output 3, a 25% chance of both exiting through output 4, and a 50% chance of them splitting (since there are two outcomes that produce this result, namely R-T and T-R). When we solve for the cases using Eq. (3.4), we find that the probability of both photons traveling to one detector or the other is

$$P(2_3, 0_4) = P(0_3, 2, 4) = 1/2 - |R|^2 |T|^2 \left(1 + |J|^2\right), \tag{3.5}$$

where

$$J = e^{\frac{\sigma_p^2 (t-t')^2}{2}} \tag{3.6}$$

for a Gaussian temporal profile. The probability of the photons splitting and causing a coincidence is

$$P(1_3, 1_4) = 2 |R|^2 |T|^2 \left(1 + |J|^2\right). \tag{3.7}$$

By examining Eq.(3.6) together with Eqs. (3.5) and (3.7) and assuming a 50:50 beam splitter ($|R|^2 = |T|^2 = 0.5$), it becomes apparent that if the delay between the photons $\Delta t = t - t'$ is 0, then $J = 1$. Therefore the probability of the two photons traveling to the same detector is $P(2_3, 0_4) = P(0_3, 2_4) = 0$, while the probability of them splitting and causing a coincidence count is $P(1_3, 1_4) = 1$.

We tried this setup hoping that it would eliminate distinguishability by making the photons have equal amounts of "s" and "p" polarizations and by eliminating ellipticity. We hoped that this would provide us with a clearer display of interference. In the absence of quantum effects, 50% of our pairs should split and cause coincidences, so we should see our count rate double as the probability goes to 1 (100% chance of coincidence). Examination of Fig. 3.5 reveals that our count rates only increase from about 1.75 to about 3. While this increase of 70% is more pronounced than the dip in

the first setup, it still suggests the presence of some distinguishability which remains to be discovered and eliminated. Furthermore, we still see unexpected fluctuations in the coincidence rate at 3 mm and 7.5 mm. The fact that these fluctuations occurred at the same wedge positions in both setups suggests that they may not simply be noise — there may be some anomaly in our quartz at that particular point.

3.2 Future Improvements

The first improvements that should be made to the apparatus should be to make the dip in Fig. 3.1 go lower by improving our indistinguishability. The first thing to try would be re-aligning the variable quartz delay with both polarizers horizontal to attempt to reduce the coincidence counts. While we did already attempt this, alignment is a very tedious process and it is possible that further effort could lead to success.

Unfortunately, with the beam splitter as it is, the interference dip will never go to zero. There are two ways that this could probably be fixed. The first would be to "randomize" the polarization of the photons with respect to the beam splitter so that we can get a 50:50 transmission ratio (see the "random polarization" line in the graph in Fig. 3.2). If a 1/2 wave plate for 916 nm light could be obtained, this would allow the polarization to be rotated 45°. Thus the photons would have equal amounts of "s" and "p" polarizations with respect to the beam splitter. The second method would simply be to purchase a better beam splitter that gets closer to a 50:50 transmission ratio, regardless of the polarization of the incident light. Either of these methods should work to make the dip go lower or all the way to zero, but both would require extra funding to buy components.

We could also improve the setup in Fig. 3.4 by obtaining better detectors which

can register an arrival of a "double" photon packet — two photons arriving at exactly the same time. This improvement would allow measurement of both coincidences and doubles, so it would be possible to observe a drop in doubles as our coincidences reach their peak. However, these photon detectors are extremely costly, and probably won't be available to us any time soon.

The best way to improve our experiment would be to increase our coincidence counts. This would allow the acquisition of statistically significant data in less time (one of the graphs above took several hours to scan, which would be impractical in a classroom setting), and it would also decrease the problem of noise. Increasing our counts could be accomplished by removing surfaces or components which eliminate part of our signal. For example, if we could replace the two prisms in the fixed-width delay with one piece of quartz, we would eliminate two interfaces. Since each interface reflects about 4% of our signal, this would increase our count rate by about 8%. We could also achieve higher count rates by purchasing a thicker BBO crystal, but this would also broaden our dip.

One of the biggest improvements that can be made in the future would be acquisition of a new laser. Diode lasers at 405 nm are now available, but purchasing one will require considerably more funding. Replacement of the laser would require purchasing a new crystal and new bandpass filters (since the photon pairs created would be 810 nm instead of 916 nm), but it would dramatically increase our counts due to the efficiency of the photon detectors. At 916 nm, the detectors register about 20% of the photons that strike them (see Fig. 3.7 [9]). This means that we are only seeing about 4% of the coincidences that are really there. If we could change to 810 nm light, our efficiency would increase to about 55%, meaning that we would then see about 30% of the coincidences produced. This would increase our coincidence rate by a factor of six.

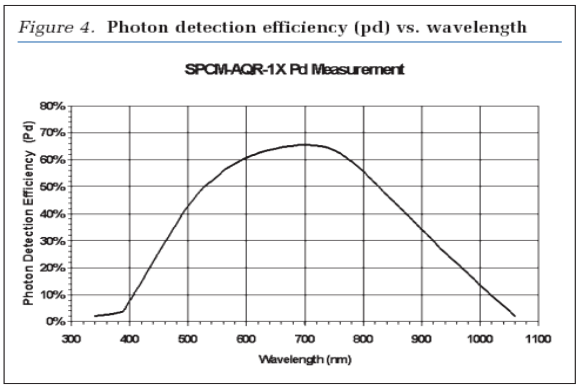

Figure 3.7 A plot from the data sheet for the photon detectors [9] showing the detection efficiency as a function of wavelength.

Chapter 4

Conclusion

We successfully constructed a two particle interferometer using parametric downconversion as a source of entangled photon pairs. Using the interferometer we were able to create entangled photon pairs and observe a statistically significant change in event rates, corresponding to interference, when distinguishability was minimized. In the first setup we observed a decrease in coincidence detection rates, which correspond to photon pairs splitting at the beam splitter and traveling to different detectors, as we varied the temporal delay between the two photons. In the second setup we observed an increase in coincidence counts, indirectly indicating a decrease in doubles counts, which correspond to photon pairs being reflected or transmitted together when entering the same input arm of a beam splitter. The first setup demonstrated destructive quantum interference of two events, whereas the second setup demonstrated constructive interference of those same two events.

Despite our successful observation of quantum interference, however, future improvements remain to be made. Although we were able to observe a statistically significant change in event rates, we were only able to observe a change of about 45% in the first setup and about 70% in the second, instead of the 100% change

which should be observed in both. This data suggests that we have been unable as yet to completely eliminate distinguishability from our setup, and therefore the two photons are not interfering perfectly. Furthermore, the data we obtain shows more variation and takes more time than is ideal for a classroom setting. If this setup is to be applied to the undergraduate Optics and Quantum Mechanics course curriculums, improvements should be made to increase photon-pair production rates and decrease noise and distinguishability, in order to observe complete interference in less time.

Bibliography

[1] D. J. Griffiths, *Introduction to Quantum Mechanics*, 2nd ed. (Pearson, Upper Saddle River, NJ, 2006), pp. 433–434.

[2] R. Lange, J. Brendel, E. Mohler, and W. Martienssen, "Beam Splitting Experiments with Classical and with Quantum Particles," Europhysics Letters **5,** 619–622 (1988).

[3] C. K. Hong, Z. Y. Ou, and L. Mandel, "Measurement of Subpicosecond Time Intervals between Two Photons by Interference," Phys. Rev. Lett. **59,** 2044–2046 (1987).

[4] A. V. Sergienko, Y. H. Shih, and M. H. Rubin, "Experimental evaluation of a two-photon wave packet in type-II parametric downconversion," J. Opt. Soc. Am. B **12,** 859–862 (1995).

[5] D. Branning, A. L. Midgall, and A. V. Sergienko, "Simultaneous measurement of group and phase delay between two photons," Physical Review A 62 (2000).

[6] N. Terry, "Production of Correlated Photon Pairs through Laser Downconversion in a BBO Crystal," Masters Thesis (Brigham Young University, Provo, UT, 1999).

[7] D. Niemi, "Observation of Entangled Photons Produced in Laser Downconversion," Senior Thesis (Brigham Young University, Provo, UT, 2004).

[8] N. Instruments, "NI 660x User Manual," http://www.ni.com/pdf/manuals/372119a.pdf (Accessed July 20, 2007).

[9] P. Elmer, "Photon detector efficiency curves," http://optoelectronics.perkinelmer.com/content/Datasheets/DTS_SPCMAQR.pdf (Accessed July 23, 2007).

[10] C. O. Components and Accessories, "Dispersion Equations for Optical Materials," http://www.cvilaser.com/Common/PDFs/Dispersion_Equations.pdf (Accessed July 20, 2007).

[11] J. Peatross and M. Ware, *Physics of Light and Optics* (Brigham Young University, Provo, UT, 2006), p. 96.

[12] C. B.-B. Borate, β BaB2O4, and BBO, "NI 660x User Manual," http://www.castech-us.com/casbbo.htm (Accessed July 20, 2007).

[13] Thorlabs, "Non-Polarizing Plate Beamsplitters Transmission Curves," http://www.thorlabs.com/NewGroupPage9.cfm?ObjectGroup_ID=915 (Accessed July 22, 2007).

[14] R. Louden, *The Quantum Theory of Light*, 3rd ed. (Oxford Science, New York, 2000), pp. 261–264.

Index